

## Kinetic Pathways of Lamellae to Gyroid Transition in Weakly Segregated Diblock Copolymers

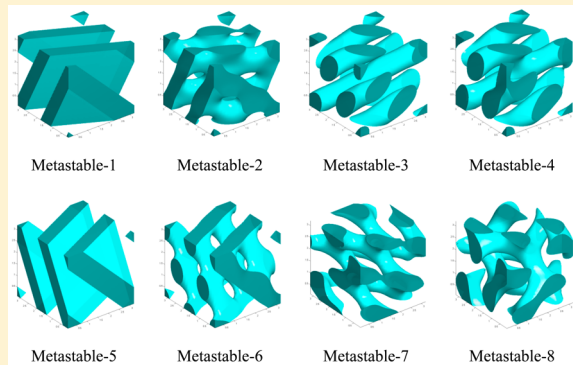
Nan Ji, Ping Tang\*, and Feng Qiu\*

State Key Laboratory of Molecular Engineering of Polymers, Key Laboratory of Computational Physical Sciences, Collaborative Innovation Center of Polymers and Polymer Composite Materials, Department of Macromolecular Science, Fudan University, Shanghai 200433, China

An-Chang Shi

Department of Physics and Astronomy, McMaster University, Hamilton, Ontario, Canada L8S 4M1

**ABSTRACT:** The kinetic pathways connecting the lamellar and gyroid phases in weakly segregated block copolymers are examined by combining the string method and the self-consistent mean-field theory for polymers. In particular, phase transition from arbitrarily oriented lamellae to gyroid is studied. The results reveal that initially the lamella will evolve into a metastable structure via a nucleation and growth mechanism, and then a secondary nucleation of the gyroid occurs in the metastable phase. The observed metastable structures include the perforated lamellae (PL), the O<sup>70</sup> phase, and the tetragonally perforated layers (TPL<sub>abc</sub>). Nucleation and growth is the dominant mechanism, and prior phase transition passed by HPL<sub>abc</sub>, which is a long-lived metastable structure, has the minimal energy barrier.



### I. INTRODUCTION

As a classical self-assembly system, block copolymer melts and solutions with periodic ordered mesophases have been the focus of intense research for many years.<sup>1–6</sup> Conventional phase structures, including lamellae (L), hexagonally packed cylinders (H), body-centered cubic spheres (C), and complex structures such as the gyroid (G) and O<sup>70</sup> phases, have been identified in simple linear diblock copolymers.<sup>4,7–10</sup> In addition to these stable morphologies, interesting metastable structures, such as the hexagonally perforated layers (HPL), are also observed in experiments.<sup>2,11</sup> Beyond the simple linear AB diblock copolymers, multiblock copolymers composed of more chemically distinct blocks and block types provide a much larger parameter space with a boundless array of possible structures. With the appearance of more stable or metastable mesophases, the dynamics of order–order (OOT) and order–disorder (ODT) phase transitions should present a challenging topic for theoretical study. Because of their long-chain nature, block copolymer melts exhibit large relaxation times in phase transformation, which makes the mechanism of their phase transition richer and more interesting. Furthermore, the study of the OOT or ODT mechanism in block copolymers is helpful in designing suitable processing routes for fabrication of specific and well-ordered structures.<sup>12</sup>

The study of OOT and ODT extends beyond block copolymers. For example, surfactant solutions undergo similar OOT as a function of the temperature and concentration.

Examples of the OOT include H–G,<sup>8</sup> L–G,<sup>13–17</sup> L–H,<sup>18</sup> and C–H transitions.<sup>19,20</sup> A common feature of these phase transitions is that the two ordered phases usually exhibit epitaxial relations;<sup>21–23</sup> i.e., the periodic structural elements of one mesophase grow from the structural elements of the other. In particular, the epitaxial relationship between the L and G phases was first observed in the surfactant C<sub>12</sub>E<sub>6</sub> (C = methylene or methyl, E = oxyethylene)/water system. Rançon and Charvolin concluded that the (211) planes of the G phase are epitaxially related to the (001) planes of the L phase and the (10) planes of the H phase.<sup>24</sup> They attributed this relationship to the fact that these planes have the highest density of material in the three phases. They also demonstrated that the H-cylinders grow parallel to the [111]-direction of the G phase. Schulz et al. confirmed that the same mechanism occurs in block copolymer mixture systems.<sup>8</sup> Hamley et al. also found that the (211) reflections of the G phase develop from the (001) reflection of the L planes in the melt of a poly(oxyethylene)–poly(oxybutylene) (PE–PB) diblock copolymer.<sup>15</sup> The metastable or intermediate structures on the kinetic pathway such as perforated layers (PL) and hexagonally perforated layers (HPL) were observed by using scattering techniques, transmission electron microscopy, and rheological measurements. The two

**Received:** September 15, 2015

**Revised:** November 11, 2015

**Published:** November 19, 2015



HPL structures found were HPL<sub>ab</sub> (*p*6<sub>3</sub>/*mmc*) with ABAB two-layer stacking and HPL<sub>abc</sub> (*R*3*m*) with ABCABC three-layer stacking. In addition to the traditional phase transition process, the relationship between the ordered bicontinuous double diamond (OBDD) structure and the G phase is also investigated in recent years. Chu et al. showed an OBDD structure in a slightly asymmetric syndiac poly(propylene)-poly(styrene) block copolymer as-cast from xylene,<sup>25</sup> and the OBDD structure transformed into the G phase when heated. Seddon et al. examined the epitaxial relationship between OBDD and G in lipid glycerol monooleate.<sup>26</sup> They concluded the phase transition from OBDD to G with two coexisting orientations, with the ⟨100⟩ and ⟨111⟩ axes parallel to the symmetry axis. Considering these previous works, it can be concluded that the epitaxial relationship exists extensively in OOT.

Among the different phase transition processes, the lamellae-gyroid (L-G) transition presents an interesting transition pathway because of the existence of metastable phases. As a representative complex structure in block copolymers, the G phase with the *Ia*3*d* symmetry has been intensively investigated for several decades. Most of the experimental observations concluded that the transition from the L to G phase in melts proceeds via intermediate PL structures.<sup>13–17</sup> These intermediate structures are long-lived nonequilibrium states which would finally convert to the bicontinuous G morphology after sufficient annealing. In general, by shearing the sample, large-scale ordered structures would appear. It was speculated that an intermediate PL with a hexagonal in-plane packing is obtained by large-amplitude shear rather than being an intrinsic feature of the structure.<sup>11,27</sup> The L-G transition in block copolymer samples without shearing could occur via a PL without hexagonal in-plane packing. The structural feature of this PL phase is a combination of L-like and G-like characteristics.<sup>11</sup> Meanwhile, without shear, different types of PL morphologies could grow in the same sample, thus leading to PL structures with apparently poor spatial order.<sup>27,28</sup> Furthermore, the HPL phase may be controlled by dislocation movements under mechanical shear, and none of the trigonal twins or hexagonal structure is in equilibrium. However, a highly regular HPL structure has been adopted spontaneously without any applied perturbing fields.<sup>29</sup> In the surfactant/water systems, a geometrical consideration shows that large deformations of HPL planes are necessary to form the double G structures (DG) from the HPL<sub>abc</sub> structure, whereas the transition from a HPL<sub>ab</sub> structure to the double G structure is straightforward.<sup>30</sup> Despite these progresses, the phase transition kinetics involving these structures and the relationship between L, PL, and G phases is still an open question.

In general, phase transition proceeds via one of the two possible mechanisms: nucleation and growth and spinodal decomposition. In block copolymer systems, most of the OOTs are first-order phase transitions. Thus, in many cases the phase transitions proceed via a nucleation and growth mechanism. However, a detailed experimental study of the critical nuclei is a difficult task. On the theoretical side, kinetics of the OOT of block copolymers has been extensively studied.<sup>12,5</sup> Laradji et al.<sup>31</sup> investigated the OOTs, such as L-H and H-C in block copolymers, by taking into account the Gaussian fluctuations and suggested that the experimentally observed modulated or perforated layers on the L-H phase boundary are a consequence of the infinitely degenerated fluctuation modes of the L phase. Subsequently, the H-G/H-C low-energy pathways on the Landau free energy surface were found and their spinodal limits obtained.<sup>32,33</sup> Matsen<sup>32</sup> suggested that the H-G transition

proceed epitaxially by a nucleation and growth mechanism. Beyond the mean-field theory, direct numerical simulation based on the time-dependent Ginzburg-Landau (TDGL) equation also gives a kinetic phase diagram for conventional structures (L-H, L-C, and H-C).<sup>34</sup> After a sudden temperature jump, transition from the L to the H phase could go through a PL intermediate state. Theoretical studies on nucleation and growth kinetics were limited until now. The size of the critical droplet of stable H-cylinders from a metastable L phase and the nucleation barrier were first determined by the nucleation theory based on a Landau-type expansion.<sup>35</sup> Critical droplets of size 30–400 cylinders with aspect ratios of 4–10 and nucleation barriers of 30–40 *k*<sub>B</sub>T are typically found. Kinetic study based on the mode expansion method has revealed that on the pathway from L to G an O<sup>70</sup> (*Fddd*) structure is a metastable intermediate.<sup>36</sup>

Recently the string method has been used to investigate the kinetic pathways of phase transitions. Previous work demonstrates that the string method provides a powerful technique to explore the free energy landscape. This method proceeds by evolving a string to converge to the minimal energy paths (MEP) connecting the initial and final states in the configuration space.<sup>37,38</sup> The nucleation of various ordered phases in block copolymers has been studied by the string method recently.<sup>37</sup> Cheng et al.<sup>37</sup> investigated the nucleation of various ordered phases in block copolymers by examining the MEP of the system. The shape, size, and free energy barrier of the critical nucleus were obtained from the MEP, providing information about the emergence of a stable ordered structure from a metastable phase. Li et al.<sup>39</sup> also studied metastability and removal mechanisms of prototypical dislocation or jog defects of lamella-forming copolymers by the string method recently. Using a similar strategy, Wang et al.<sup>40</sup> demonstrated the optimal epitaxies between ordered phases are always related to the minimal nucleation barrier. They concluded that the epitaxial relation originates from the matching of the dominant Fourier components of the density distribution. The results also confirm that string method is very useful for the block copolymer self-assembling studies.

In this work we combine string method and the self-consistent field theory (SCFT) to investigate the kinetic pathways of the L-G transition. We focus on the nucleation and growth mechanism, in which a nucleus of the new phase grows locally, and the spinodal decomposition, in which the old phase evolves gradually to the new phase. Through this method, we obtain the free energy landscape for the transition from L to G. We systematically studied the epitaxial relationship and several metastable states between L and G phases. In particular, the one-step mechanism and two-step mechanism are distinguished. The details of the nucleation and growth of the PL structure and G phase are presented. The result will help to understand the kinetic relationship among L, G, and PL phases.

## II. THEORY AND COMPUTATION METHOD

**A. Self-Consistent Field Theory.** Our method starts with the polymeric SCFT, which has been widely used in thermodynamic and morphological studies of polymeric systems. In what follows we will present a brief introduction of the theoretical framework and leave the details to the literature.<sup>38</sup> We consider an incompressible system of *n* AB diblock copolymers in a volume *V*. All the chains are assumed to have the same degree of polymerization *N*, and the volume fraction of the A species is *f*. In the self-consistent field theory, the many interacting chains are reduced to that of independent chains subject to an external

(mean) field, created by the other chains. The fundamental quantity to be calculated is the polymer segment probability distribution function,  $q(\mathbf{r}, s)$ , representing the probability of finding segment  $s$  at position  $\mathbf{r}$ . It satisfies a modified diffusion equation which is based on a flexible Gaussian chain model:

$$\frac{\partial q(\mathbf{r}, s)}{\partial s} = \frac{1}{6} b^2 \nabla^2 q(\mathbf{r}, s) - [\gamma_A(s)\omega_A(\mathbf{r}) + \gamma_B(s)\omega_B(\mathbf{r})]q(\mathbf{r}, s) \quad (1)$$

where  $b$  is the Kuhn length of the polymer segment and  $\omega_K(\mathbf{r})$  is the self-consistent field representing the interaction exerted to the species  $K$ , and  $\gamma_K(s)$  is 1 if  $s$  belongs to block  $K$  and 0 otherwise. The initial condition of the above equation is  $q(\mathbf{r}, 0) = 1$ . Because the two ends of the diblock chain are distinct, a second end-segment distribution function is  $q^*(\mathbf{r}, s)$  needed. It satisfies eq 1 only with the right-hand side multiplied by  $-1$ , and the initial condition,  $q^*(\mathbf{r}, N) = 1$ . Accordingly, the partition function of a single chain subject to the mean field,  $\omega_K(\mathbf{r})$ , can be written as  $Q = (1/V) \int d\mathbf{r} q(\mathbf{r}, s) q^*(\mathbf{r}, s)$  in terms of  $q(\mathbf{r}, s)$  and  $q^*(\mathbf{r}, s)$ .

With the above description, the free energy functional of the system is given by

$$\begin{aligned} \frac{F}{nk_B T} = & -\ln Q + \frac{1}{V} \int d\mathbf{r} [\chi N \varphi_A(\mathbf{r}) \varphi_B(\mathbf{r}) - \omega_A(\mathbf{r}) \varphi_B(\mathbf{r}) \\ & - \omega_B(\mathbf{r}) \varphi_A(\mathbf{r}) + \xi(\mathbf{r})(1 - \varphi_A(\mathbf{r}) - \varphi_B(\mathbf{r}))] \end{aligned} \quad (2)$$

where  $\chi$  is the Flory–Huggins interaction parameter between A and B species,  $\varphi_A(\mathbf{r}) = (V/NQ) \int_0^N ds q(\mathbf{r}, s) q^*(\mathbf{r}, s)$  and  $\varphi_B(\mathbf{r}) = (V/NQ) \int_0^N ds q(\mathbf{r}, s) q^*(\mathbf{r}, s)$  are the local volume fractions (or, equivalently, the local density distribution) of A and B, respectively.  $\xi(\mathbf{r})$  is the potential field that ensures the incompressibility of the system. Minimization of the free energy functional with respect to the fields in eq 2 leads to a set of self-consistent equations. Their solutions can be obtained by using the powerful pseudospectral method originally proposed by Rasmussen et al.<sup>41,42</sup>

**B. String Method.** Once the free energy of the system is obtained, the next step is to use it as an input for the string method. The purpose of the string method is to find the MEP  $\psi$  on the energy landscape. A MEP is a curve (string) in the configuration space, connecting two states X and Y (usually named the ends of the string), which satisfies

$$\nabla F(S)^\perp \psi = 0 \quad (3)$$

where  $\nabla F^\perp$  is the component of  $\nabla F$  normal to the string  $\psi$  and  $S$  (string) is a parameter differentiating the different phases of the system. The states (including morphology and free energy) at the two ends of the string, such as the stable L and G phases, can be obtained by simply solving the SCFT at appropriate conditions.<sup>4</sup> Other initial states on the string (or pathway) are set up by a combination of the two end states, which is described as follows: Taking the L–G transition as an example, if the transition process is through the nucleation and growth mechanism, initially the G-nucleus will be formed in the middle of the computation box and the rest volume of the box is occupied by the L-planes. Thus, the initial density distribution of this system on the string is set to be

$$\varphi_{R_{nu}}^i(\mathbf{r}) = \varphi_G(\mathbf{r}) \quad (|r - r_c|^2 < R_{nu}^2) \quad (4)$$

$$\varphi_{R_{nu}}^i(\mathbf{r}) = \varphi_L(\mathbf{r}) \quad (|r - r_c|^2 > R_{nu}^2) \quad (5)$$

where  $\mathbf{r}_c$  is the central point of the box and  $R_{nu}$  is the radius of the initial spherical G-nucleus.  $R_{nu}$  is linearly increased from 0 to  $D/2$  to screen the critical nucleus, where  $D$  is the side length of the computation cubic box.

For possible transition pathways via the spinodal mechanism, in which the density distribution evolves simultaneously in the whole space, the initial density distribution of a state on the string is set to be a gradual change in the whole box from L to G:

$$\varphi_j^i(\mathbf{r}) = \varphi_L(\mathbf{r}) + \frac{j}{M} (\varphi_G(\mathbf{r}) - \varphi_L(\mathbf{r})), \quad j = 0, 1, \dots, M \quad (6)$$

where  $M$  is the total number of states on the string.  $\varphi_0^i(\mathbf{r}) = \varphi_L(\mathbf{r})$  and  $\varphi_M^i(\mathbf{r}) = \varphi_G(\mathbf{r})$  are the density distribution of the L and G structures at the two ends of the string, respectively. The parameter  $S$  ranges from 0 to 1:

$$S(\text{string})_j = \frac{\sum_r (\varphi_j^i(\mathbf{r}) - \varphi_L(\mathbf{r}))^2}{\sum_r (\varphi_G(\mathbf{r}) - \varphi_L(\mathbf{r}))^2} \quad (7)$$

After all the initial states are set up, the state of the system is then iterated by using SCFT. After several iteration steps, the states are adjusted by the differential method to obtain numerical solutions of dynamics (eq 3). After full relaxation, the shape of the string is fixed and the minimum free energy path is obtained.

The nucleus of a phase is defined by a pointwise phase-density function:<sup>37</sup>

$$\Phi_S(\mathbf{r}) = \frac{|\varphi(\mathbf{r}) - \varphi_m(\mathbf{r})|}{|\varphi(\mathbf{r}) - \varphi_m(\mathbf{r})| + |\varphi(\mathbf{r}) - \varphi_S(\mathbf{r})|} \quad (8)$$

$$|\varphi(\mathbf{r}) - \varphi'(\mathbf{r})| = \int d\mathbf{r}' w(\mathbf{r}' - \mathbf{r}) [\varphi(\mathbf{r}') - \varphi'(\mathbf{r}')]^2 \quad (9)$$

where  $w(\mathbf{r})$  is the mollifier with the form

$$w(\mathbf{r}) = C e^{R^2 / (|\mathbf{r}|^2 - R^2)} \quad (R > 0) \quad (10)$$

Then the boundary between the different phases can be specified by set  $\Phi_S(\mathbf{r}_{BD}) = 0.5$ , where  $\mathbf{r}_{BD}$  is the position of the boundary.

### III. RESULTS AND DISCUSSION

To simplify the calculation, we have fixed the A-block fraction to be  $f = 0.41$  and investigated in the weak segregation region by choosing the Flory–Huggins parameter  $\chi N = 12–14$ . The SCFT simulations show that the system with these parameters is in a stable G phase region. At first the initial and final structures at the end of the string are found by solving the SCFT equations for the L and G phases. For each phase, by minimizing its free energy with respect to the cubic box size  $D$ , the characteristic length scale of the phase or the optimized box size in unit of the radius of gyration of the block copolymer ( $R_g$ ) is determined. The entire string is discretized into 20 or 40 points (each point corresponding to a state with specific morphology). After full relaxation of the string the MEP, corresponding to the pathway of the structure evolution, is obtained.

#### A. One-Step Nucleation and Growth Mechanism.

**A1. Epitaxial Relationship.** In general, to simulate phase transitions proceeding through a nucleation and growth mechanism, a large enough calculation box is required. In our calculation, without losing the key feature of the nucleation process, the system size is chosen to be 27 times that of the smallest cell. All of the lamellae and gyroid phase are in the same coordinate system. The initial states are L planes with different

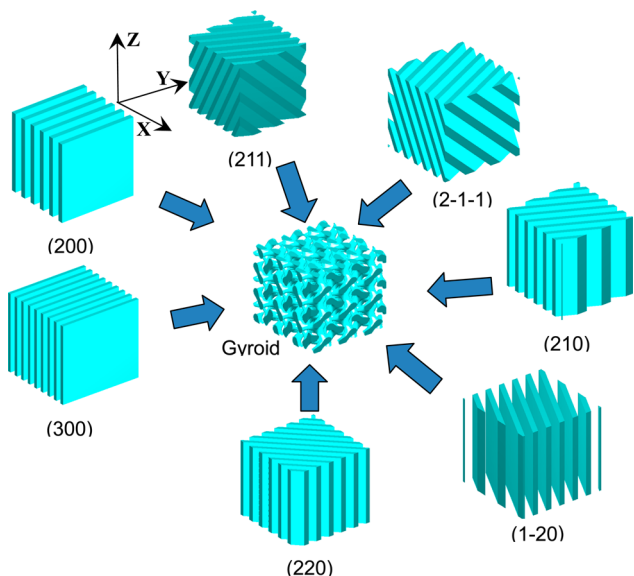
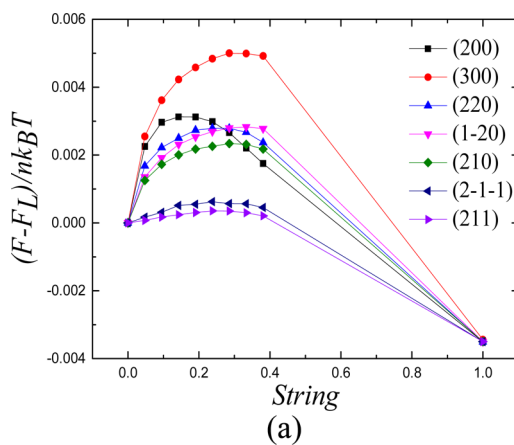


**Figure 1.** Initial states: lamella phases with various orientations and the final gyroid phase.

orientations and the final gyroid with a fixed orientation (Figure 1). Interestingly, the L phase with (211) planes has almost the same box size  $D$  with that of the G phase along the [001] direction. This is also one of the key evidence showing there is an epitaxial relationship between these two structures.

The minimal free energy pathways starting from various L planes to the G phase are shown in Figure 2. When the free energy reaches its maximum, the critical nucleus of the G phase can be obtained. Figure 3 shows the structure of critical nucleus of gyroid in lamella with different wave vectors, and Figure 4 shows the order parameter profiles of the central nucleus from a perspective view along the layer during the evolution from L to G. It is clear that the pathway starting from the (211) L planes has the lowest energy barrier as compared with the others. In this case, the lowest free energy barrier of a single block copolymer is  $3.5 \times 10^{-4} k_B T$ , which is an order of magnitude lower than that in the other pathways. This suggests that the epitaxial relationship between L and G is indeed the (001) plane of L to (211) plane of G. The reason is that the critical nucleus of the G phase with (211) plane along the layer is the easiest to grow in the L phase.



(a)

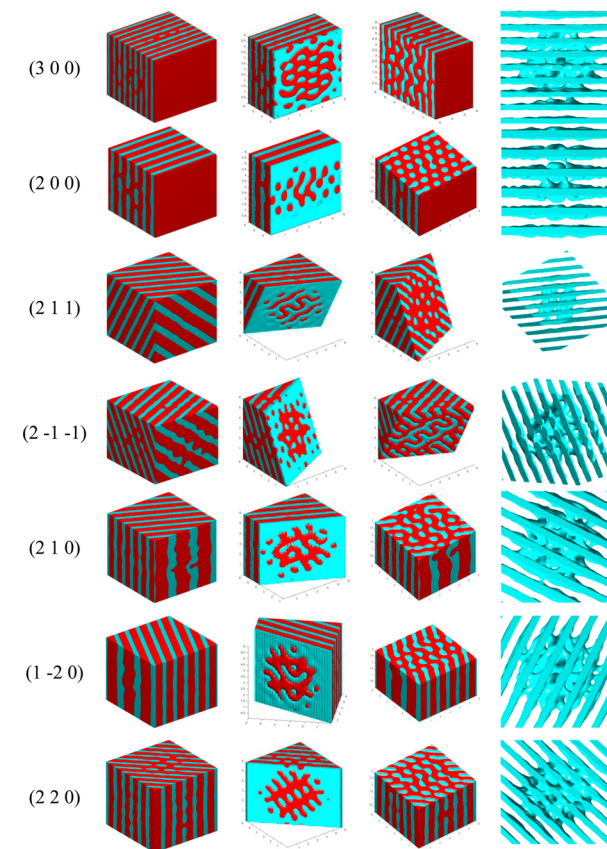
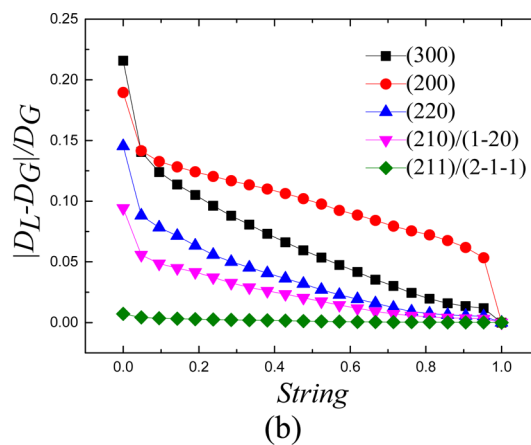


**Figure 3.** Critical nucleus of gyroid in lamella with different wave vectors.

The volumes of the G-critical nucleus are about  $(2-5) \times 10^3 (R_g^3)$  under current conditions. Both of these volumes and the energy barriers for the G-critical nucleus formation in different pathways are shown in Table 1 along with the corresponding optimized box size  $D$  (characteristic length of each phase). Because the phase transition occurs close to the order-disorder boundary ( $\chi N = 12.5$ ) and the energy barrier for single block polymer is about  $10^{-3} k_B T$ , this may be affected by thermal fluctuation. We will discuss this issue later.



(b)

**Figure 2.** Phase transition process from lamellae to gyroid with nucleation and growth mechanism at  $f = 0.41$  and  $\chi N = 12.5$ . (a) Free energy along the minimal energy pathway for the phase transition. The latter part of the string is ignored. (b) Characteristic box size along the minimal energy pathway for the phase transition.

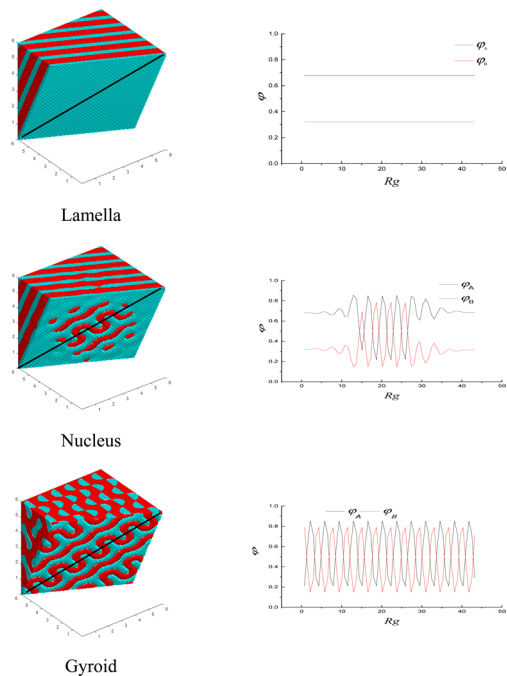


**Figure 4.** Order parameter profiles of the cross section along the black line of the central nucleus. The three structures are lamella (211), gyroid nucleus in the lamella, and gyroid, respectively.

**Table 1. Lamellae with Different Wave Vectors**

	$(D_x, D_y, D_z) (R_g)$	free energy barrier ( $k_B T$ )	vol of nucleus ( $R_g^3$ )
L (300)	(30.6, 25.17, 25.17)	0.00 500 221	4954.69
L (200)	(20.4, 25.17, 25.17)	0.00 312 208	1986.79
L (211)	(24.99, 24.99, 24.99)	0.00 035 452	3768.00
L (2-1-1)	(24.99, 24.99, 24.99)	0.00 062 348	3773.75
L (210)	(22.8, 22.8, 25.17)	0.00 233 717	4268.30
L (1-20)	(22.8, 22.8, 25.17)	0.00 282 728	5012.81
L (220)	(28.83, 28.83, 25.17)	0.00 278 996	4235.86
gyroid	(25.17, 25.17, 25.17)		

The G phase has a set of {211} fundamental reciprocal lattice vectors, which can be classified into two groups, each with six vectors. Although we can set 12 L structures initially, there are only two kinds of minimal energy pathways. So we choose (211) and (2-1-1) as the representative for each group. The free energy barrier of phase transition from L with (211) plane is 3.5

$\times 10^{-4} k_B T$ , while from L with (2-1-1) plane is  $6.2 \times 10^{-4} k_B T$ . Although the free energy barriers of these two processes are different, compared to starting from other planes, such as (220) or (210), they can be assumed the same. Since both the L with (211) plane and that with (2-1-1) plane have the same optimized box size which is  $24.99 \times 24.99 \times 24.99 R_g^3$ , the domain spacing match should be more important than orientation in an epitaxial transition. Indeed, previous theoretical study found that H  $\leftrightarrow$  C epitaxial phase transitions in block copolymers also show a good domain spacing match.<sup>33</sup> If the phase periodicity is constant in the phase transition, polymers only experience a local rearrangement. Conversely, if the phase periodicity is mismatched, the phase transition should need a macroscopic transport of materials. The variations of the box sizes along the phase transition pathways starting from different L plane orientations to fixed G phase orientation are shown in Figure 2b. The L with the (211) plane has a small mismatch with the G phase (<1%), so an epitaxial phase transition would be easy to occur. The box sizes of other L phases with different orientations all have a large mismatch (>10%). The larger the mismatch is, the higher the free energy barrier in the transition pathway. Furthermore, for a bigger mismatch (>10%), usually the optimized box size changes significantly at first as shown in Figure 2b, and then the phase transition proceeds gradually. We note that Matsen has obtained similar conclusions in a study of the phase transition from H to C phase.<sup>33</sup>

It is known that the symmetry of a classic gyroid structure is constituted by (211) and (220) plane series. The phase transition from lamellae to gyroid is thought of existing epitaxial relationship by many works. They found that the (001) plane of lamellae is epitaxially related to the (211) plane of the gyroid in assembling systems.<sup>24,15</sup> However, the real phase transition process is a nucleation and growth one. The nucleation and growth mechanism of OOT in block copolymer system has comparatively few studies. Kinetics and evolving grain structures of diblock copolymers during OOT are more studied such as the nucleation, growth rates, shapes, and types of block copolymer grains. Among them, nucleation is most interesting. Nucleation and growth is considered to be the phase transition mechanism from lamellae to gyroid by many experimental works. Like previous work, we also carry out a detailed study about this epitaxial relationship with nucleation and growth mechanism by the string method.

**A2. Free Energy Barrier.** Figure 5 shows the minimal free energy pathway of phase transition through a nucleation and

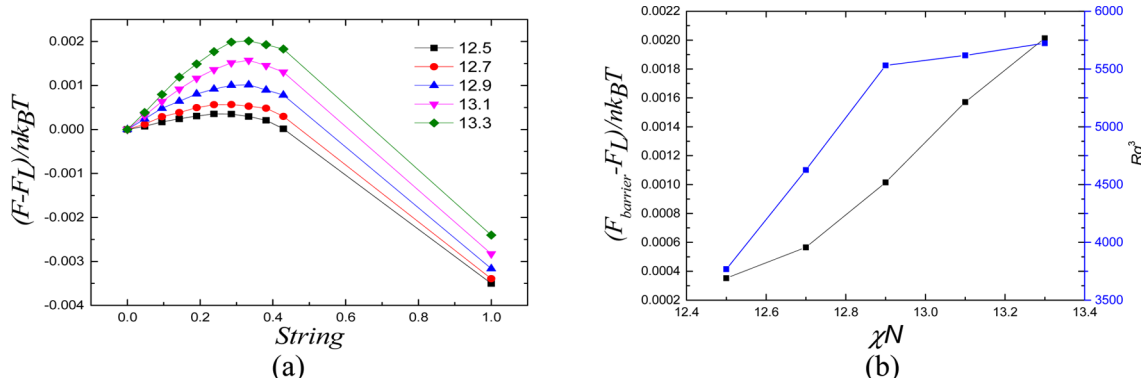


**Figure 5.** (a) MEP from lamellae to gyroid via nucleation and growth mechanism at  $\chi N = 12.5–13.3$ . (b) The corresponding nucleus volume and free energy barrier per nucleus with varying  $\chi N$  values.

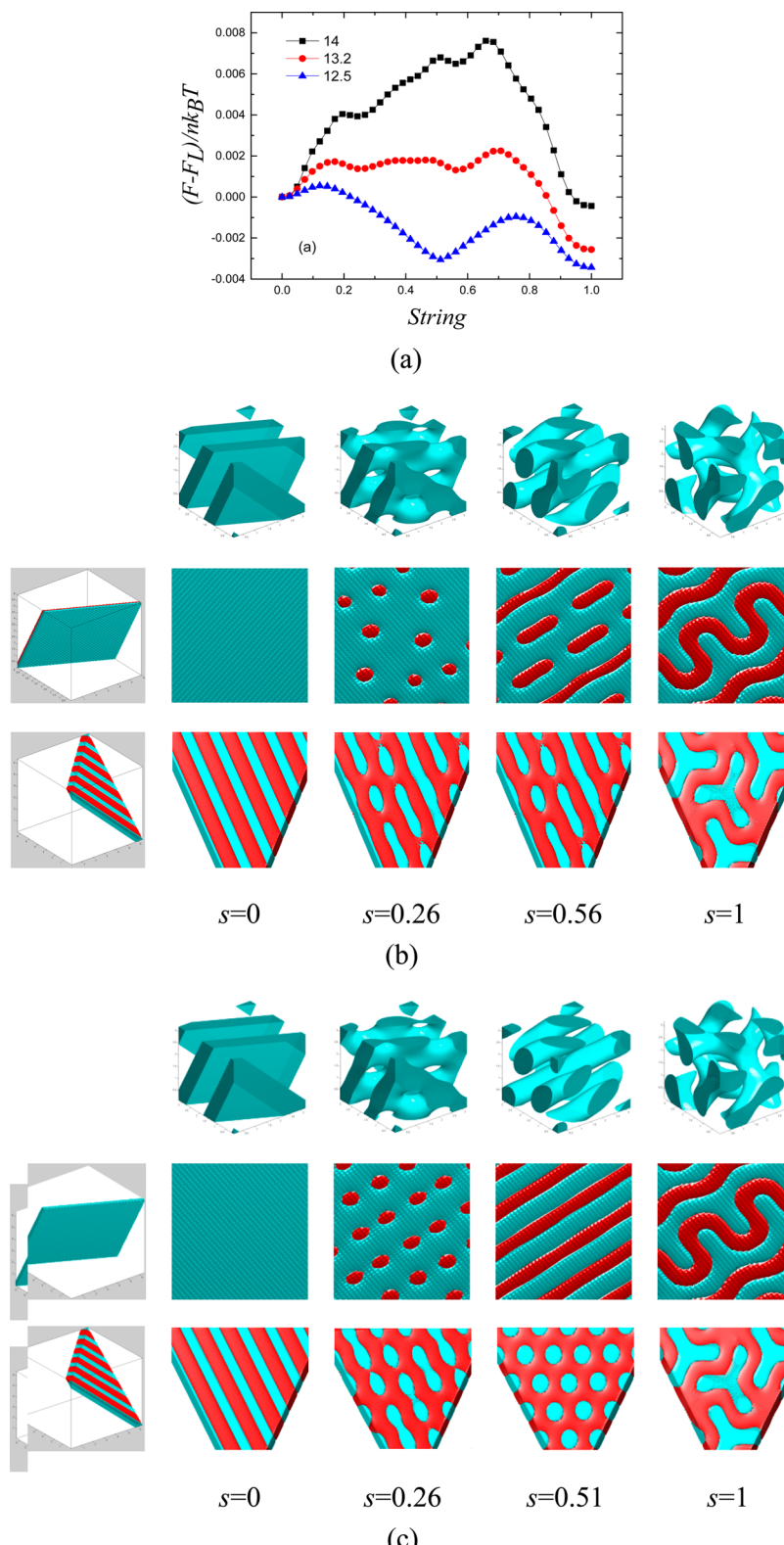


**Figure 6.** Phase transition processes for screening the metastable structures. The initial structure is lamella with {211} wave vector from gyroid. The cross sections are (211) plane (parallel to the layer) and (1–1–1) plane (perpendicular to layer). (a) Minimal free energy pathway for screening the metastable structures with  $\chi N = 12.5/13.2/14$ . (b) Morphologies on the minimal free energy pathway with  $\chi N = 14$ . (c) Morphologies on the minimal free energy pathway with  $\chi N = 12.5$ .

growth mechanism from L to G with different  $\chi N$  values. As  $\chi N = 12.5$ , the free energy barrier per chain is  $3.5 \times 10^{-4} k_B T$ , and it becomes higher with increased  $\chi N$ . As  $\chi N$  is increased to 13.3, the free energy barrier per chain reaches  $2.01 \times 10^{-3} k_B T$ , almost an

order of magnitude higher. In experiment, direct measurement of the free energy barrier is very difficult. Usually the kinetic data from time-resolved small-angle X-ray scattering (tr-SAXS) or rheological measurement are analyzed by the Avrami equation:

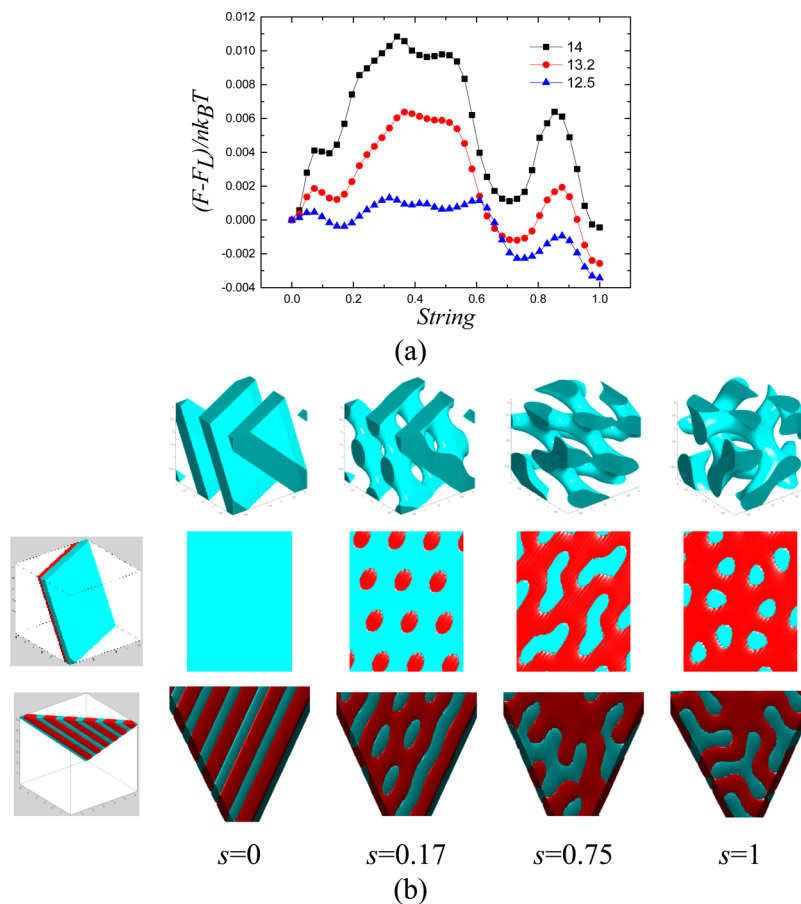


**Figure 7.** Phase transition processes for screening the metastable structures. The initial structure is lamella with {2–1–1} wave vector from gyroid. The cross sections are (2–1–1) plane (parallel to the layer) and (111) plane. (a) Minimal free energy pathway for screening the metastable structures with  $\chi N = 12.5/13.2/14$ . (b) Morphologies on the minimal free energy pathway with  $\chi N = 12.5$ .

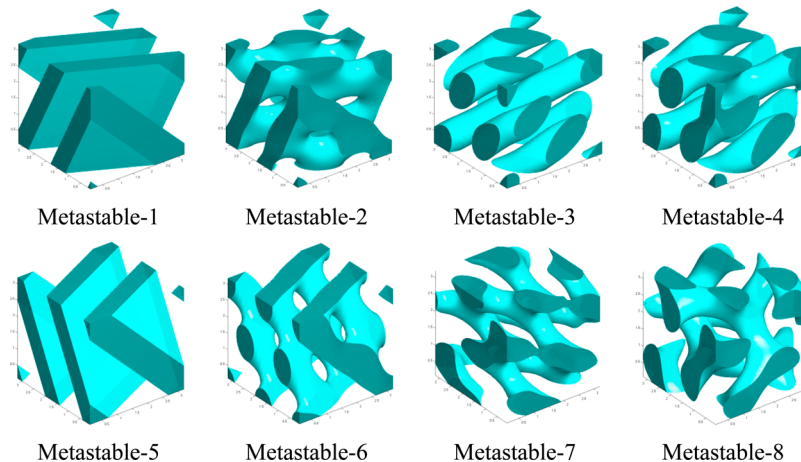


**Figure 8.** All of the stable and metastable morphologies on the phase transition pathway from lamella to gyroid.

$$\varphi_G(t) = 1 - e^{-kt^n} \quad (11)$$

where  $\varphi_G(t)$  is the volume fraction of the gyroid phases at time  $t$ ,  $n$  an integer which reflects the nature of the transformation, and  $k$  the rate constant of the phase transition.

Floudas et al. studied the kinetics of the H–G, H–L, and L–G transitions using this method.<sup>43</sup> They found the H–G transition involves the nucleation and highly anisotropic growth of the G phase along the cylinder axis, and it is a highly cooperative process ( $\sim 50$  kcal/mol). However, such experiment is easily

influenced by the defects and the complex external conditions. In a theoretical study, Wickham et al.<sup>35</sup> examined the L–H transition through the nucleation and growth mechanism by using the Landau–Brazovskii model for diblock copolymer melts. It is found that the nucleation barrier is  $30\text{--}40k_B T$  in the weak segregation region for diblock copolymers. Since the segment volume is  $Na^3$  for a single diblock chain, the number of the chains in a critical nuclei is  $v_N N^{1/2}/6^{3/2}$  where  $v_N$  (in unit of  $R_g^3$ ) is the volume of the critical nuclei. From our calculation, it is seen that the volume of the critical nuclei becomes larger with

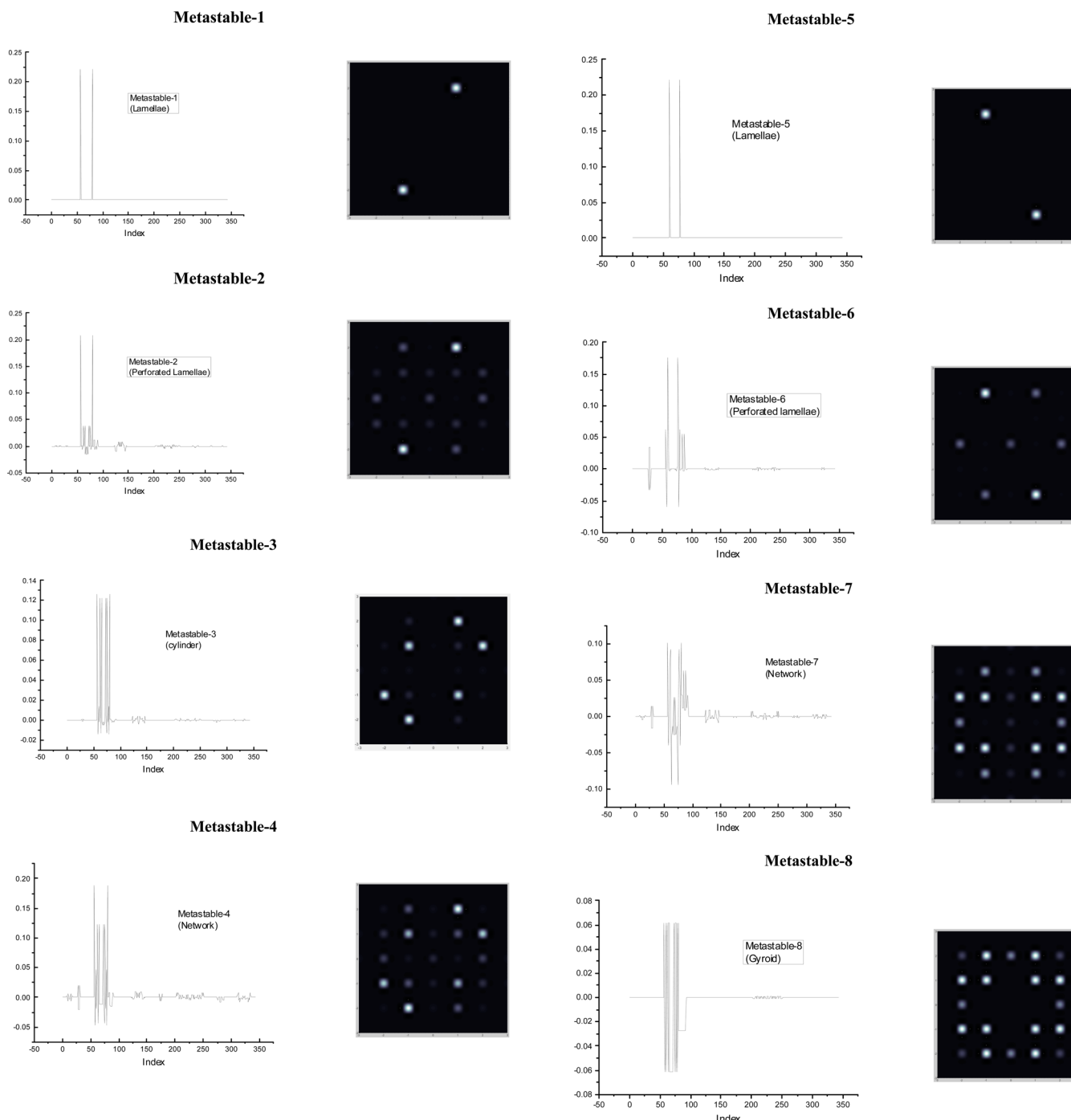


**Figure 9.** Spectral analysis of all initial phases and metastable structures. The left side is the result of discrete Fourier transform of the density distribution. The right side is the corresponding two-dimensional projection along the  $z$  direction.

increased  $\chi N$ . When  $\chi N$  is greater than 12.9, the volume of the critical nuclei varies smoothly. Considering such variation and assuming the degree of polymerization to be  $10^4$ , the free energy barrier is estimated to be from 9.1 to  $78k_B T$  with  $\chi N$  varying from 12.5 to 13.3. Thus, our results are also consistent with previous predictions based on nucleation theory.

Within the mean-field theory thermal fluctuations are ignored. Because the molecular chain of polymer is usually very long, fluctuation effects are suppressed and SCFT could have accurate results. However, near the ODT fluctuation effects could not be ignored. Fredrickson and Helfand investigated the effect of composition fluctuations of microphase separation in diblock

copolymer system.<sup>12</sup> The location of the ODT is predicted to be at  $\chi N = 10.495 + 41.022\bar{N}^{-1/3}$ , where  $\bar{N}$  is the invariant polymerization index. Therefore, only if  $\bar{N} > 8000$ , the phase transition which we studied as  $\chi N = 12.5$  will not be in a disorder area.

**B. Two-Step Nucleation and Growth Mechanism.** *B1. Identifying Possible Metastable Structures.* According to previous experiments for diblock copolymer melts, metastable structures on the OOT pathway from L to G phase can be classified into two main types: perforated layer (PL) and network (NW) structures. Using the method mentioned in the Theory

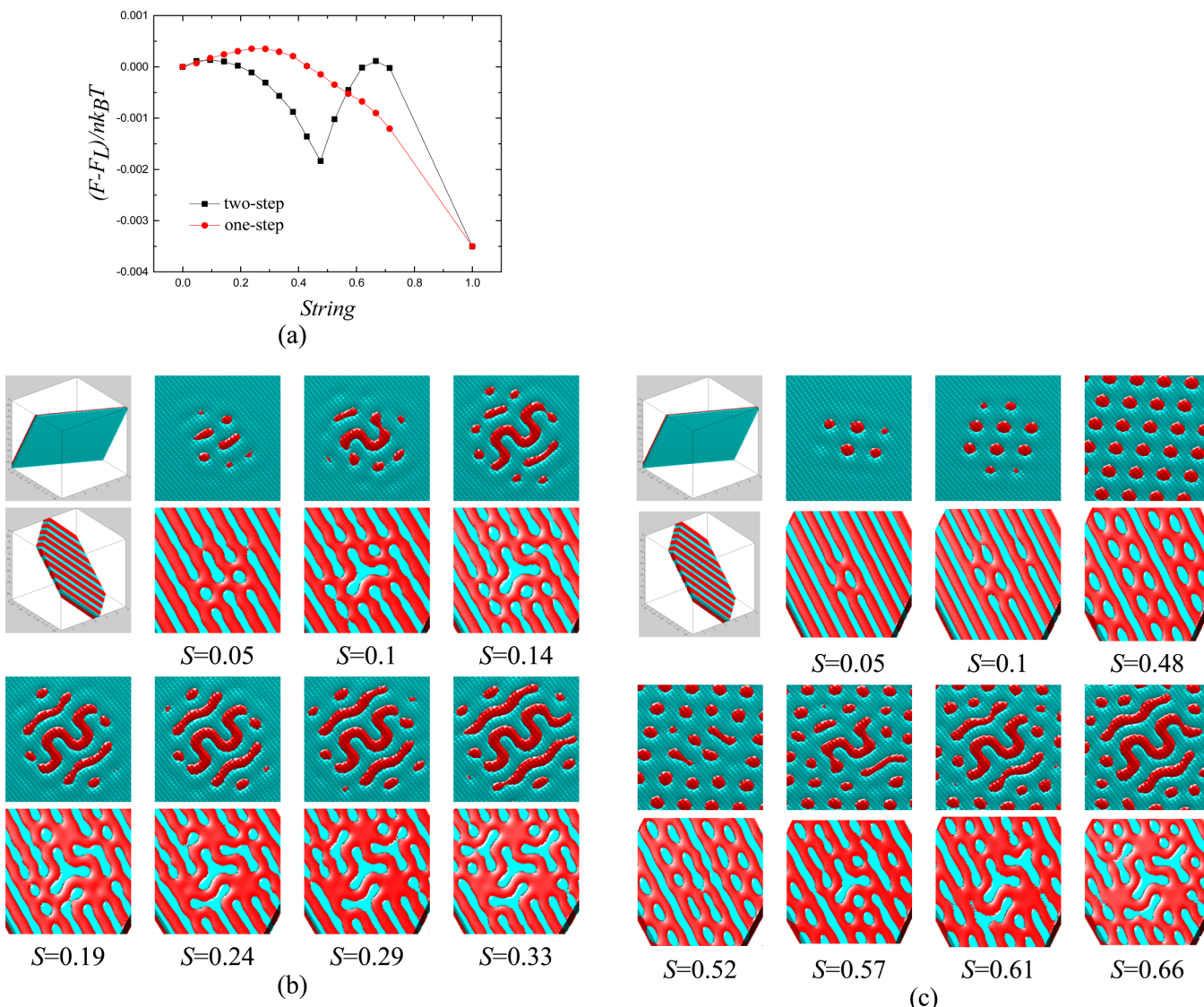


**Figure 10.** Phase transition processes from lamella to gyroid with nucleation and growth mechanism. The initial structure is lamella with {211} wave vector gyroid coordinate. The cross sections are (211) plane (parallel to the layer) and (111) plane. (a) Minimal free energy pathway of phase transition with one-step (L-G) nucleation and two-step nucleation (L-PL-G) as  $\chi N = 12.5/13.2/14$ . (b) Morphologies on the minimal free energy pathway with one-step nucleation. (c) Morphologies on the minimal free energy pathway with two-step nucleation.

and Computation Method section, we are able to scan possible metastable structures along the transition pathways.

We first study the phase transition processes from L with different planes such as (211) or (2-1-1) to G phase. The optimized box sizes of the L structure with (211) or (2-1-1) plane are  $D = 8.3/8.5/8.8$  as the Flory-Huggins parameter  $\chi N$  is 12.5/13.2/14, respectively. When  $\chi N = 14$ , it is already very close to the phase boundary between L and G phases; while  $\chi N = 12.5$ , it is close to the phase boundary between H and G. The entire string is discretized into 40 states. As we mentioned in the Theory and Computation Method section, for searching possible metastable structures, in overall space the density of the initial structures on the pathway is gradually evolved. After full relaxation, a metastable structure could be found. The results for the phase transition process from L to G phase are shown in Figures 6 and 7. It is clear that the transition from the initial L phase with (211) plane has the lower free energy barrier than that with (2-1-1) plane. The free energy barrier per chain is  $5.4 \times 10^{-4} k_B T$  for  $\chi N = 12.5$ , which is greater than that through the

nucleation and growth mechanism. This further confirms that the nucleation and growth mechanism is what happens in the real experiment. Detailed phase transition process of metastable structures with a two-step nucleation mechanism will be discussed later.

It is seen from Figures 6 and 7 that the free energy barrier decreases with the decrease of  $\chi N$ , and at least two barriers exist between the L and G phases, suggesting the existence of metastable structures. The valleys on the free energy curve correspond to metastable structures. In particular, as shown in Figure 6 in the phase transition starting from the initial L with the (211) plane, if the phase transition occurs close to the L stable region ( $\chi N = 14$ ), two metastable structures are observed at  $S = 0.26$  and  $S = 0.56$ , respectively, in which the free energy barrier is the highest; while if the phase transition happens in the area close to the H phase ( $\chi N = 12.5$ ), only one metastable structure is obtained at  $S = 0.51$ . In contrast, for the phase transition from L with the (211) plane, there are always two metastable structures.

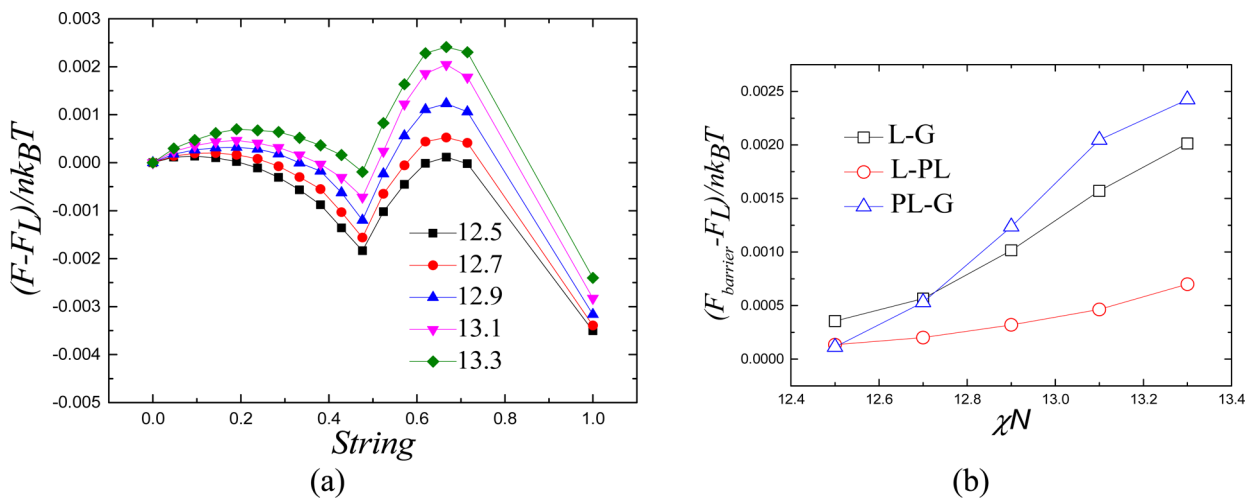


**Figure 11.** (a) MEP from L to G via PL. The Flory–Huggins parameters  $\chi N$  is from 12.5 to 13.3. (b) The corresponding free energy barrier of various phase transition pathways.

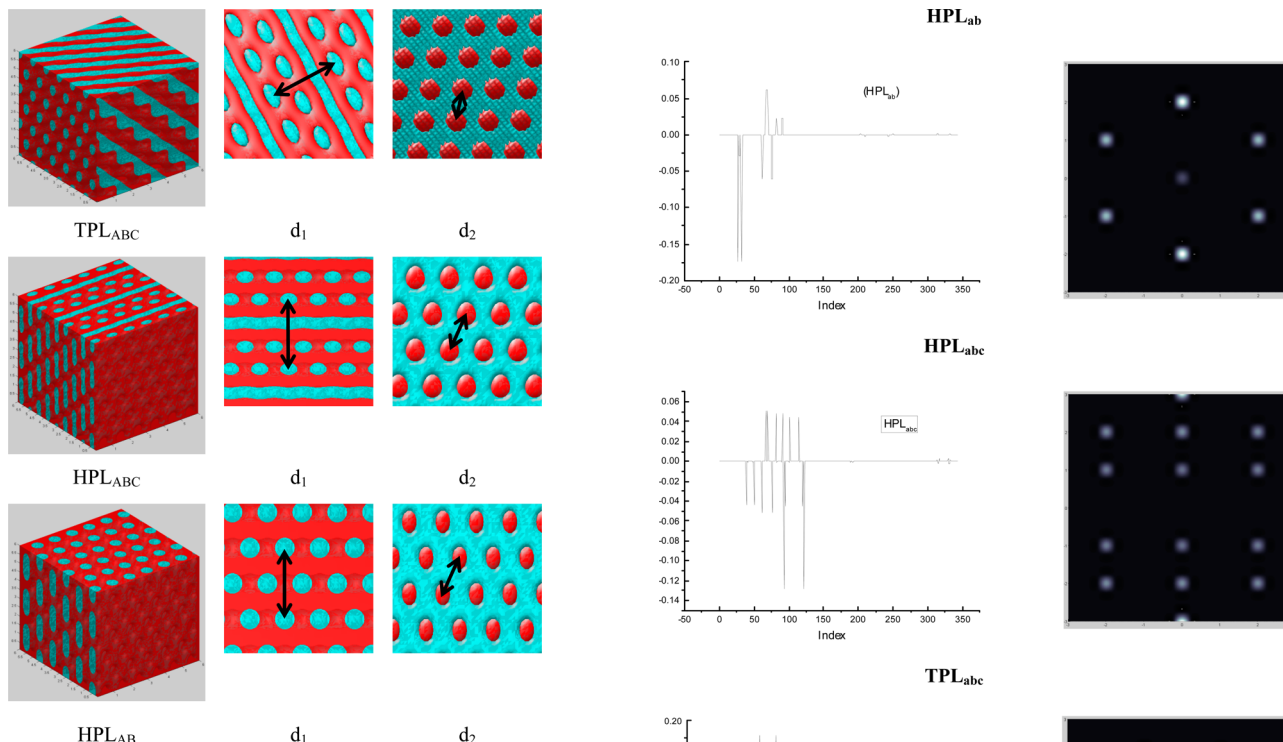


**Figure 12.** Perforated layer structures: tetragonally perforated layer with ABC stacking ( $TPL_{ABC}$ ), hexagonally perforated layer with ABC stacking ( $HPL_{ABC}$ ), and hexagonally perforated layer with AB stacking ( $HPL_{AB}$ ).  $d_1$  is repeat spacing perpendicular to the plane of lamella.  $d_2$  is repeat spacing along the plane of lamella.

For  $\chi N = 12.5$ , they are found at  $S = 0.17$  and  $S = 0.75$ , respectively, as shown in Figure 7.

**B2. Metastable Structures.** All the metastable structures observed as well as the stable L, H, and G phases are summarized in Figure 8. Discrete Fourier transforms of these metastable structures are shown in Figure 9. It is obvious that Metastable-2 ( $S = 0.26$  in Figure 6b) and Metastable-6 ( $S = 0.17$  in Figure 7b) are PL structures, which means that L always passes by the PL structure first in the pathway from L to G phase. Metastable-3 ( $S = 0.51$  in Figure 6c) is hexagonally ordered cylinders (H) phase, while in Metastable-4 ( $S = 0.56$  in Figure 6b), three cylinders are

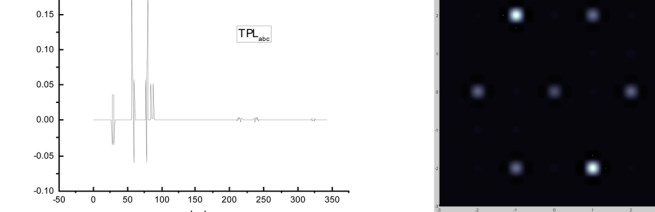


**Figure 13.** Spectral analysis of three perforated lamella phase. The left side is the result of discrete Fourier transform of the density distribution. The right side is the corresponding two-dimensional projection along the  $z$  direction.

connected together by the coordinated junctions. This cylinder-like structure is similar to the metastable state which appears in a SCFT study of the transition from H to G.<sup>32</sup> Both the axes of H and the cylinder-like structure orient along the diagonal direction  $[-1-11]$  of the computation box, which is consistent with the

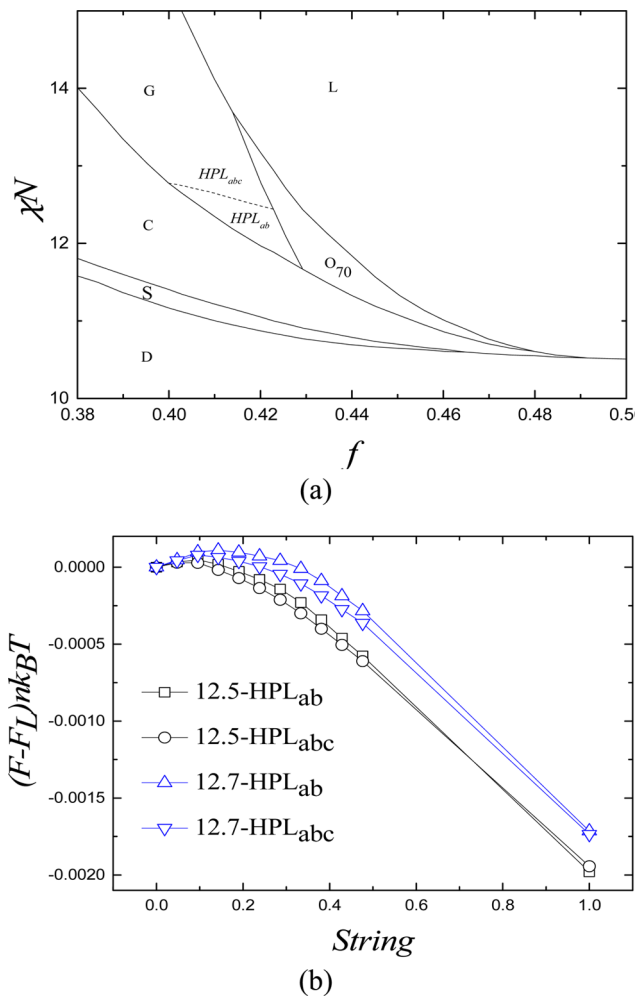


**Figure 14.** Phase transition from lamella to perforated layer with nucleation and growth mechanism. The perforated layer structures: hexagonally perforated layer with ABC stacking ( $HPL_{ABC}$ ); hexagonally perforated layer with AB stacking ( $HPL_{AB}$ ). (a) The phase diagram with unstable perforated layer structures. (b) The MEP from lamella to perforated layer structures with  $\chi N = 12.5$  and  $\chi N = 12.7$ .

experimental results.<sup>8</sup> This is an indication showing that the cylinder-like structure is also possible to appear on the L–G transition pathway, although this phase transition takes place far away from the H stable region. Conversely, the hexagonally cylinder will appear. The minority A-domain in Metastable-7 ( $S = 0.75$  in Figure 7b) forms a network constructed from 3-fold coordinated junctions within the B-matrix, which is very similar to the  $O^{70}$  structure.

The epitaxial relationship between L and G phases is shown in Figures 6 and 7. The cross-section pictures of the metastable structures in Figures 6b and 6c and Figure 7b show the L–G epitaxy more clearly. Positions of the hole in PL are determined by the structural characteristics of the G phase. Taking the two metastable structures in the transition processes in Figure 6 as an example, at first the holes start to appear on the lamellae, then these holes grow bigger gradually, and the structure becomes cylinder-like. At last, the cylinder-like structure break apart leaving a series of 3-fold junctions characteristic of G phase. All of the complex HPL-like and cylinder-like structures combine a 3-fold-coordinated minority component domain structure similar to that of the G morphology with the layered characteristic of the

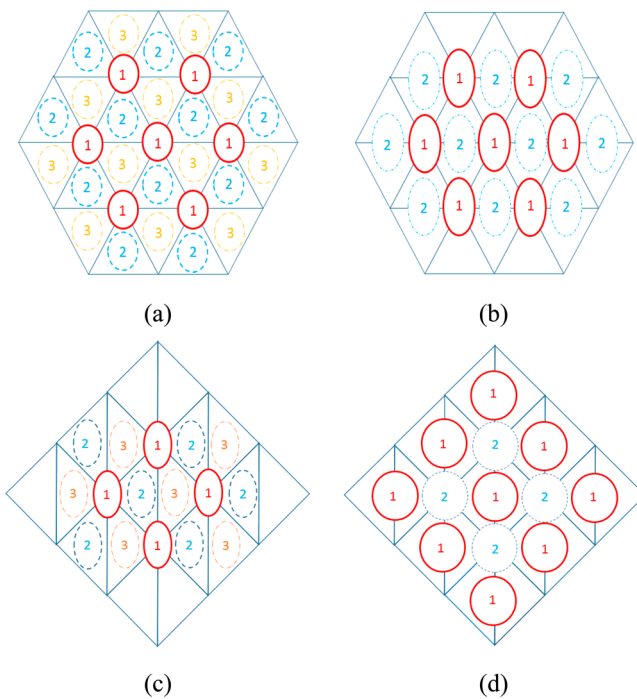


**Figure 15.** Perforated layer phase in weakly segregated diblock copolymers. “1, 2, 3” represent the different layers in the structures. (a) Hexagonally perforated layer  $HPL_{abc}$  phase. (b) Hexagonally perforated layer  $HPL_{ab}$  phase. (c) Tetragonally perforated layer  $TPL_{abc}$  phase. (d) Tetragonally perforated layer  $TPL_{ab}$  phase.

L plane. The H cylinders grow parallel along the (1–1–1) plane of the G phase.

Complex network metastable structures are also observed on the pathway of other experimental systems. Squires et al. suggested a mechanism whereby the transformation from L to QIIg proceeds via an intermediate phase, which they suggested is the diamond inverse bicontinuous cubic phase (QIID).<sup>45</sup> Yamada et al. investigated the dynamics of ODT and OOT for block copolymers by solving a set of amplitude equations derived from the TDGL equation.<sup>36</sup> They believed the  $O^{70}$  ( $Fddd$ ) structure is a metastable entrance of G phase. In our calculation, we have received a total of two metastable NW structures. Note that the Metastable-7 ( $S = 0.75$  in Figure 7b) has the significant structural feature of  $O^{70}$ : it has a 3-fold coordinated lattice. The structure which we are most interested in is Metastable-4 ( $S = 0.56$  in Figure 6b). It is a cylinder-like structure in which each three adjacent columns are connected together. The cylinder-like structure is similar to the metastable phase which appears in the transition from H to G. We believe it is a metastable entrance of G phase, too.

We noted that in our calculation the PL with accurate hexagonal symmetry in plane and (211) plane could not been obtained due to the limitation by the cubic box. The HPL structure plays an important role on the kinetic pathway from L to G phase. Zhu et al. investigated the OOT of the polystyrene-*b*-poly(ethylene oxide) (PS-*b*-PEO) diblock copolymer in reciprocal space by small-angle X-ray scattering (SAXS) and in real space by transmission electron microscopy (TEM).<sup>27,28</sup> Their results suggest that the epitaxy relationships for the HPL–DG transformation could be recognized as the (100)  $HPL_{ab}$ –(112) DG, the (120)  $HPL_{ab}$ –(220) DG, and the (001)  $HPL_{ab}$ –(111) DG. However, the perforation of the hexagonal structure should rearrange itself first, followed by the perforation in the

trigonal structure from G phase. Imai et al. concluded that large deformations of HPL<sub>abc</sub> planes are necessary to form the DG structure, whereas the transition from a HPL structure with ABAB stacking to the DG structure is straightforward.<sup>17</sup> We believe that the PL with in-plane hexagonal packing will not appear spontaneously, but is induced by the shearing field, although results from other experiments on complex copolymer systems show the HPL structure without shearing. We also found the PL without in-plane hexagonal packing could appear directly on the L–G phase transition pathway.

**B3. Free Energy Barrier.** With the metastable structures obtained, we further study the L–G phase transition pathway via these metastable structures. Two different transition processes have been identified, as shown in Figure 10. On the pathway with higher free energy barrier, G phase is nucleated directly in L phase. In this process, the free energy barrier per chain is  $3.5 \times 10^{-4} k_B T$  with the corresponding string length being 0.25. In the other pathway with lower free energy barrier ( $1.35 \times 10^{-4} k_B T$  per chain, and the corresponding string length is 0.05), the PL nucleus appears first on the pathway. Only after the holes spread all over the space, the G phase nucleation begins to take place, which corresponds to a string length of about 0.5. As the string length goes to 0.66, a free energy barrier of  $1.13 \times 10^{-4} k_B T$  per chain is reached. The two-step nucleation mechanism further validates the appearance of the metastable PL structure in experiment. However, here the holes in the layers arrange not hexagonally but tetragonally. The reason may be that in computation all the structures on a pathway are always confined in a cubic box. But a perfect hexagonal structure should have different domain sizes with L and G phases. The details of the PL will be discussed later. The morphology of the nuclei is also shown in Figure 10. The nuclei of the PL structure in the L phase are small; their volume is  $2621.3 R_g^3$ . The volume of the G-nuclei in PL is  $4979.2 R_g^3$ , which is also larger than the G-nuclei in the L phase.

The cross-section pictures of the morphologies on the nucleation and growth pathway are shown in Figures 10b and 10c. In the one-step process shown in Figure 10b, at the beginning near the G-forming nuclei there are growing holes, whose locations are determined by the final G structure. Later larger pores gradually fuse together to form the G nuclei. In the two-step process shown in Figure 10c, a few holes appear on the L planes at first. After the formation of the PL structure at  $S = 0.48$ , there is a minimum of the free energy. Then several holes show up again and the G-nucleus starts to emerge. The process exhibits an epitaxy which explains the low activation barrier. These results are in excellent agreement with a recent SCFT calculation by Zhang et al.<sup>37</sup> Floudas et al. also studied the kinetics of the H–G, H–L, and L–G transitions by using synchrotron SAXS and rheometry.<sup>43</sup> The G–L transition was found to contain a double nucleation and growth mechanism: first, the H structure nucleates in the G phase, and then the L structure nucleates in the H phase, which is consistent with our inference.

The free energies along the phase transition pathways by the two-step nucleation and growth mechanism for different  $\chi N$  are shown in Figure 11. When  $\chi N > 12.7$ , the free energy barrier with the two-step nucleation and growth mechanism will be higher than that with the one-step mechanism. However, the barrier of transition from L to PL is always lower than the other two transitions.

**C. PL Structures.** The complex PL structure is an interesting phase. From the experiments,<sup>44,45</sup> the HPLs ( $p6_3/mmc$ ) and

( $R\bar{3}m$ ) are known to be long-lived metastable structures in diblock copolymer melts. However, the Metastable-2 and Metastable-6 we obtained have no perfect hexagonal symmetry. Structural features of Metastable-2 are the combination of L-like and G-like characteristics. Perforations in these complex-PLs are combined by two kinds of staggered arrangement modes. The Metastable-6 in Figure 8 has a clear BCC in-plane packing. So we name it tetragonal perforated layer (TPL) structure.

In order to compare with the result of previous experiment, we also study phase transition kinetics from L to PL through the nucleation and growth mechanism. When  $\chi N = 12.5$ , a TPL<sub>abc</sub> structure is found. Three ordered PL structures as the ends of the strings are TPL<sub>abc</sub>, HPL<sub>ab</sub>( $p6_3/mmc$ ), and HPL<sub>abc</sub>( $R\bar{3}m$ ), respectively, as shown in Figure 12. Discrete Fourier transforms of three perforated lamellae are also shown in Figure 13. Using the SCFT theory, Matsen examined the stability of the HPL<sub>abc</sub> and HPL<sub>ab</sub> structures.<sup>46</sup> For  $\chi N \leq 13$ , the HPL<sub>ab</sub> structure is more stable than the HPL<sub>abc</sub> structure, whereas for  $\chi N > 13$ , their relative stability reverses. As a comparison, we found HPL<sub>abc</sub> is stable than the HPL<sub>ab</sub> structure for  $\chi N \geq 12.7$  as  $f = 0.41$ . The free energy of these structures and the free energy barrier of the phase transition processes are shown in Figure 14. Figure 14a is the phase diagram with metastable HPL structures. The free energy of HPL<sub>ab</sub> is less than that of HPL<sub>abc</sub>. As  $\chi N = 12.5$ , the L–G phase transition process occurs in the G stable region but near the G–H boundary. The height of the free energy barrier along the L–PL transition pathway has the order: HPL<sub>abc</sub> ( $R\bar{3}m$ ) < HPL<sub>ab</sub> ( $P6_3/mmc$ ) < TPL<sub>abc</sub>, thus transforming into HPL<sub>abc</sub> experiences the lowest barrier. Note that the free energy of HPL<sub>abc</sub> itself is higher than that of HPL<sub>ab</sub> when  $\chi N = 12.5$ .

The topology of the PL structures deserves a careful investigation, in which only the stacking sequence of HPL structure has been clearly understood. A PL structure can be identified by the ratio of two repeat spacing: the repeat spacing of layers ( $d_1$ ) and holes ( $d_2$ ), which are sketched in Figure 15.

In fact, Loo et al. have analyzed the ratio  $d_1/d_2$  according to their SAXS patterns.<sup>29</sup> They found the  $d_1/d_2$  ratio of HPL<sub>abc</sub> is 2.24, which is quite similar to that found by Zhu et al. (which is 2.13) in a shear-oriented polystyrene/poly(ethylene oxide) diblock copolymer,<sup>27,28</sup> and the ratio of HPL<sub>ab</sub> is 1.58. We also studied the ratio  $d_1/d_2$  with accurate calculation and found it to be 2.61 for HPL<sub>abc</sub>, 1.88 for HPL<sub>ab</sub>, and 2.15 for TPL<sub>abc</sub>. Our result is a little bigger than that of the experiments. Figure 15 shows all the proposed PL structures, including HPL<sub>abc</sub>, HPL<sub>ab</sub>, TPL<sub>abc</sub>, and TPL<sub>ab</sub>. The structures are based on our calculations except TPL<sub>ab</sub>, in which the numbers (1, 2, 3) represent the different layers, respectively. As the effect of entropy, holes of every layers are staggered as much as possible. Therefore, we believe that the shapes of the holes in each structure are not the same. Holes are oval in TPL<sub>abc</sub> and HPL<sub>ab</sub>. Although the TPL has never been reported before in block copolymers, we believe it is very likely to exist (although only in a metastable state).

#### IV. CONCLUSIONS

The L–G phase transition pathways in weakly diblock copolymer are systematically investigated by combining the string method and polymer SCFT. We focus on the nucleation and growth mechanism of the phase transition. In addition, the string method is extended to analyze the epitaxial relationship between the ordered mesophases. The results reveal various epitaxial relationships between lamella and gyroid mesophases. The phase transition of lamella with (211) planes to gyroid has a minimal free energy barrier. We observe two kinds of metastable phases

existing between lamella and gyroid: perforated layer and complex network structures. Some of the metastable perforated layer structures without in-plane hexagonal packing combine a 3-fold-coordinated minority component domain structure similar to that of the gyroid morphology with the layered characteristic of the lamellae one, while some of the metastable perforated layer structures have a clear BCC in-plane packing. However, the perforated layer structures with in-plane hexagonal packing ( $HPL_{abc}$ ) almost has the lowest energy. The nucleation and growth is the preferred mechanism of the phase transition, which is a complex two-step nucleation mechanism between lamellae and gyroid. The nucleus of the perforated layers appears first on the pathway with lower free energy barrier. After the holes spread all over the space, the nucleation of the gyroid phase takes place. This mechanism is in agreement with the results of previous experiments. We also propose the detailed structures of the perforated layers based on the calculation. The method we developed could be widely used in studying the order-order phase transition kinetics.

## AUTHOR INFORMATION

### Corresponding Authors

\*E-mail pingtang@fudan.edu.cn (P.T.).  
\*E-mail fengqiu@fudan.edu.cn (F.Q.).

### Notes

The authors declare no competing financial interest.

## ACKNOWLEDGMENTS

We thank financial support from the National Basic Research Program of China (Grant 2011CB605700) and the National Natural Science Foundation of China (Grants 21320102005 and 21374023).

## REFERENCES

- (1) Leibler, L. *Macromolecules* **1980**, *13*, 1602–1617.
- (2) Thomas, E. L.; et al. *Nature* **1988**, *334*, 598–601.
- (3) Bates, F. S.; Fredrickson, G. H. *Annu. Rev. Phys. Chem.* **1990**, *41*, 525–557.
- (4) Matsen, M. W.; Schick, M. *Phys. Rev. Lett.* **1994**, *72*, 2660–2663.
- (5) Shi, A.-C.; Noolandi, J.; Desai, R. C. *Macromolecules* **1996**, *29*, 6487–6504.
- (6) Fredrickson, G. H. *The Equilibrium Theory of Inhomogeneous Polymers*; Oxford University Press: Oxford, 2006.
- (7) Hajduk, D. A.; Harper, P. E.; Gruner, S. M.; Honeker, C. C.; Kim, G.; Thomas, E. L.; Fetters, L. J. *Macromolecules* **1994**, *27*, 4063–4075.
- (8) Schulz, M. F.; Bates, F. S.; Almdal, K.; Mortensen, K. *Phys. Rev. Lett.* **1994**, *73*, 86–89.
- (9) Tyler, C. A.; Morse, D. C. *Phys. Rev. Lett.* **2005**, *94*, 208302.
- (10) Takenaka, M.; et al. *Macromolecules* **2007**, *40*, 4399–4402.
- (11) Hamley, I. W.; Koppi, K. A.; Rosedale, J. H.; Bates, F. S.; Almdal, K.; Mortensen, K. *Macromolecules* **1993**, *26*, 5959–5970.
- (12) Fredrickson, G. H.; Helfand, E. J. *Chem. Phys.* **1987**, *87*, 697.
- (13) Sakurai, S.; Umeda, H.; Furukawa, C.; Irie, H.; Nomura, S.; Lee, H. H.; Kim, J. K. *J. Chem. Phys.* **1998**, *108*, 4333–4339.
- (14) Hajduk, D. A.; Takenouchi, H.; Hillmyer, M. A.; Bates, F. S. *Macromolecules* **1997**, *30*, 3788–3795.
- (15) Hamley, I. W.; Fairclough, J. P. A.; Ryanb, A. J.; Maic, S.-M.; Boothc, C. *Phys. Chem. Chem. Phys.* **1999**, *1*, 2097–2101.
- (16) Ahn, J.-H.; Zin, W.-C. *Macromol. Res.* **2003**, *11*, 152–156.
- (17) Imai, M.; Sakai, K.; Kikuchi, M.; Nakaya, K.; Saeki, A.; Teramoto, T. *J. Chem. Phys.* **2005**, *122*, 214906.
- (18) Hamley, I. W.; Koppi, K. A.; Rosedale, J. H.; Bates, F. S. *Macromolecules* **1993**, *26*, 5959–5970.
- (19) Kimishima, K.; Koga, T.; Hashimoto, T. *Macromolecules* **2000**, *33*, 968–977.
- (20) Matsen, M. W. *J. Chem. Phys.* **2001**, *114*, 8165–8173.
- (21) Clerc, M.; Laggner, P.; Levelut, A.-M.; Rapp, G. *J. Phys. II* **1995**, *5*, 901.
- (22) Clerc, M.; Levelut, A.-M.; Sadoc, J. F. *J. Phys. II* **1991**, *1*, 1263.
- (23) Imai, M.; Kawaguchi, A.; Saeki, A.; et al. *Phys. Rev. E: Stat. Phys., Plasmas, Fluids, Relat. Interdiscip. Top.* **2000**, *62*, 6865.
- (24) Rancon, Y.; Charvolin, J. *J. Phys. Chem.* **1988**, *92*, 2646–2651.
- (25) Chu, C. Y.; Lin, W. F.; et al. *Macromolecules* **2012**, *45*, 2471–2477.
- (26) Seddon, A. M.; Hallett, J.; Beddoes, C.; et al. *Langmuir* **2014**, *30*, 5705–5710.
- (27) Zhu, L.; Huang, P.; Cheng, S. Z. D.; et al. *Phys. Rev. Lett.* **2001**, *86*, 6030.
- (28) Zhu, L.; Huang, P.; Cheng, S. Z. D.; et al. *Macromolecules* **2003**, *36*, 3180–3188.
- (29) Loo, Y. L.; Register, R. A.; Adamson, D. H.; Ryan, A. J. *Macromolecules* **2005**, *38*, 4947–4949.
- (30) Imai, M.; Sakai, K.; Kikuchi, M.; Nakaya, K.; Saeki, A.; Teramoto, T. *J. Chem. Phys.* **2005**, *122*, 214906.
- (31) Laradji, M.; Shi, A. -C.; Noolandi, J. R.; Desai, C. *Macromolecules* **1997**, *30*, 3242–3255.
- (32) Matsen, M. W. *Phys. Rev. Lett.* **1998**, *80*, 4470–4473.
- (33) Masten, M. W. *J. Chem. Phys.* **2001**, *114*, 8165–8173.
- (34) Qi, S. Y.; Wang, Z.-G. *Phys. Rev. E: Stat. Phys., Plasmas, Fluids, Relat. Interdiscip. Top.* **1997**, *55*, 1682–1697.
- (35) Wickham, R. A.; Shi, A.-C.; Wang, Z.-G. *J. Chem. Phys.* **2003**, *118*, 10293–10305.
- (36) Yamada, K.; Nonomura, M.; Ohta, T. *Macromolecules* **2004**, *37*, 5762–5777.
- (37) Cheng, X. Y.; Lin, L.; E, W. N.; Zhang, P. W.; Shi, A. C. *Phys. Rev. Lett.* **2010**, *104*, 148301.
- (38) E, W. N.; Ren, W. Q.; Vanden-Eijnden, E. *Phys. Rev. B: Condens. Matter Mater. Phys.* **2002**, *66*, 052301.
- (39) Li, W.; Nealey, P. F.; de Pablo, J. J.; Müller, M. *Phys. Rev. Lett.* **2014**, *113*, 168301.
- (40) Wang, C.; Jiang, K.; Zhang, P. W.; Shi, A.-C. *Soft Matter* **2011**, *7*, 10552–10555.
- (41) Tzeremes, G.; Rasmussen, K. Ø.; Lookman, T.; et al. *Phys. Rev. E: Stat. Phys., Plasmas, Fluids, Relat. Interdiscip. Top.* **2002**, *65*, 041806.
- (42) Rasmussen, K. Ø.; Kalosakas, G. *J. Polym. Sci., Part B: Polym. Phys.* **2002**, *40*, 1777–1783.
- (43) Floudas, G.; Ulrich, R.; Wiesner, U.; Chu, B. *Europhys. Lett.* **2000**, *50*, 182–188.
- (44) Forster, S.; Khandpur, A. K.; Zhao, J.; Bates, F. S. *Macromolecules* **1994**, *27*, 6922–6935.
- (45) Squires, A. M.; Templer, R. H.; Seddon, J. M. *Langmuir* **2002**, *18*, 7384–7392.
- (46) Matsen, M. W.; Bates, F. S. *J. Chem. Phys.* **1997**, *106* (6), 2436–244.